Steam-Oil Ratio in Steam-Solvent Coinjection Simulation for Homogeneous and Heterogeneous Bitumen Reservoirs

Arun Venkat Venkatramani
School of Mining and Petroleum Engineering,
University of Alberta,
7-203 Donadeo Innovation Centre for Engineering, 9211-116 Street NW,
Edmonton, AB T6G 1H9, Canada
e-mail: venkatra@ualberta.ca

Ryosuke Okuno[1]
Department of Petroleum and Geosystems Engineering,
University of Texas at Austin,
CPE 5.118B, 200 E. Dean Keeton Street,
Stop C0300,
Austin, TX 78712-1585
e-mail: okuno@utexas.edu

This research presents a mechanistic analysis of expanding-solvent steam-assisted gravity drainage (ES-SAGD) for heterogeneous reservoirs in terms of cumulative steam-oil ratio (SOR) as a function of cumulative bitumen production. Simulation case studies for SAGD and ES-SAGD with normal hexane at 35 bars are conducted for geostatistical realizations of two types of heterogeneous Athabasca-bitumen reservoirs. For the first type, low-permeability mudstone barriers are oriented horizontally. For the second type, they are inclined and more representative of the middle McMurray member. The solubility of water in the oleic phase at elevated temperatures is properly modeled to ensure reliable comparison between steam-assisted gravity drainage (SAGD) and ES-SAGD. Simulation results show that ES-SAGD is less sensitive to heterogeneity than SAGD in terms of cumulative SOR. On average, the reduction in SOR due to steam-solvent coinjection is simulated to be greater under heterogeneity. The reduction in SOR is greater for reservoir models with inclined mudstone barriers than in those with horizontal mudstone barriers. Analysis of simulation results indicates that the injected solvent tends to accumulate more significantly under heterogeneity, which enhances the mechanisms of ES-SAGD, such as dilution of bitumen by solvent and reduced thermal losses to the overburden. Tortuous hydraulic paths and slower gravity drainage under heterogeneity enhance the mixing between solvent and bitumen in the transverse direction along the edge of a steam chamber. Then, a larger amount of the accumulated solvent tends to facilitate lower temperatures near the chamber edge. [DOI: 10.1115/1.4040529]

Keywords: ES-SAGD, bitumen recovery, steam-oil ratio, reservoir heterogeneity, numerical simulation

1 Introduction

Steam-assisted gravity drainage (SAGD) is currently the most widely used technique for recovery of bitumen from thick reservoirs unsuitable for mining operations [1–4]. The performance of SAGD is quantified in terms of the cumulative steam-oil ratio (SOR), defined as the ratio of the cumulative steam injected cold water equivalent to the cumulative bitumen produced.

The average cumulative SOR in efficient field-scale SAGD projects is between two and five, depending on the reservoir and fluid properties [5]. In highly heterogeneous reservoirs, the average SORs are expected to be even higher due to the adverse effects of reservoir heterogeneities on hydraulic paths for fluid flow. Prior studies of SAGD in heterogeneous reservoirs indicate that the extent to which the SOR is increased under heterogeneity is sensitive to length scales of permeability barriers, and their proximity to the well pair [6–9]. Most of these studies are simulation-based, and the main permeability barriers considered is mudstone in the form of laterally extensive barriers.

Reduction of cumulative SOR is a salient engineering problem from both environmental and economic standpoints, with its economic importance enhanced under low oil prices. An effective method for lowering SAGD's SOR at a given operating pressure is by simultaneously reducing heat losses to the overburden and accelerating the drainage of the oleic phase near the chamber edge.

A widely investigated alternative to SAGD is expanding solvent-SAGD (ES-SAGD), wherein a small quantity of condensable light solvent is coinjected with steam. ES-SAGD retains many of the advantages of SAGD and can potentially lower the cumulative SOR by simultaneous reduction of operating chamber temperatures, and increase of bitumen production rate [1,10–19].

The occurrence of lower temperatures along and near the chamber edge under steam-solvent coinjection is attributed to the presence of volatile components in addition to the water and bitumen components. Vapor condensation for a given pressure occurs near the saturation temperature of water for a binary system of water and heavy hydrocarbon (e.g., bitumen as a pseudo component) [20,21]. However, it occurs at a lower temperature as the hydrocarbon component becomes lighter, as shown in the systematic experimental studies for water/hydrocarbon binaries by Brunner [22] and Brunner et al. [23]. For multicomponent mixtures of water and hydrocarbons in steam-solvent coinjection, vapor condensation occurs at the temperature for the phase transition from three phases to two phases for a given overall composition and pressure. Sheng et al. [24] presented thermodynamic calculations of this phase transition for bitumen/solvent/water mixtures for different solvent components. Their calculations and reservoir simulations consistently demonstrated that the vapor condensation

[1]Corresponding author.

Contributed by the Petroleum Division of ASME for publication in the Journal of Energy Resources Technology. Manuscript received December 2, 2017; final manuscript received May 25, 2018; published online June 26, 2018. Assoc. Editor: Ray (Zhenhua) Rui.

temperature becomes lower with increasing volatility of the solvent component in ternary mixtures of water, alkane solvent, and bitumen at a fixed overall composition and pressure.

Mobilization of bitumen in ES-SAGD mainly occurs because of the combination of temperature and dilution of bitumen by dissolution of solvent in the oleic phase (x_{sL}) within the solvent-rich liquid bank near the chamber edge. Existence of an optimal solvent volatility for successful implementation of ES-SAGD was shown in previous papers. For Athabasca bitumen reservoirs, ES-SAGD studies conducted for single component *n*-alkane solvents indicate normal hexane (*n*-C_6) to be suited [14–16,25,26].

Detailed understanding of the influence of reservoir heterogeneities on oil recovery mechanisms in ES-SAGD is necessary if its implementation is considered as a measure to lower the hurdle for development of more heterogeneous reservoirs, for which conventional SAGD is expected to be inefficient. Practical importance of such knowledge is informed by two aspects, and their effects on the cumulative SOR. First, mixing between oil and solvent is expected to be improved under permeability heterogeneity because of more tortuous hydraulic paths for fluid flow, as indicated by prior studies on miscible displacements [27–29]. Second, improved mixing between solvent and bitumen may influence the temperature distribution near the chamber edge by affecting the vaporization of solvent from the oleic phase when it interacts with steam.

Investigations into the relative performance of ES-SAGD to SAGD in the presence of reservoir heterogeneity are rather scarce. To our knowledge, Li et al. [12] is the only published mechanistic study of ES-SAGD in heterogeneous reservoirs. For synthetic reservoir models containing a single deterministically placed shale barrier at different locations, the authors showed that the recovery of oil and the accompanying SOR can be improved by coinjecting solvent with steam.

The main objective of this paper is to investigate whether ES-SAGD can be a better alternative to SAGD in highly heterogeneous bitumen reservoirs in terms of cumulative SOR as a function of cumulative bitumen production. To this end, numerical simulations for SAGD, and ES-SAGD with normal hexane as solvent (*n*-C_6 SAGD) are conducted for 100 geostatistical realizations of simple heterogeneous reservoirs comprising of Athabasca bitumen.

To our knowledge, this is the first detailed, systematic simulation study of ES-SAGD in the presence of stochastically distributed reservoir heterogeneity. This study has three main novelties: (i) ES-SAGD and SAGD are quantitatively compared in terms of cumulative SOR; (ii) the interplay among temperature, solvent-bitumen mixing near the chamber edge, and chamber geometry, and its effect on the cumulative SOR in heterogeneous reservoirs are explained; (iii) the solubility of water in the oleic phase (x_{wL}) is accurately modeled to ensure reliable comparison between SAGD and ES-SAGD on the basis of Venkatramani and Okuno [16].

Section 2 describes basic conditions used in numerical simulations in this research. Section 3 presents two simulation case studies. Section 4 summarizes the main conclusions from the case studies.

2 Basic Conditions for Simulations

2.1 Reservoir Model. Two-dimensional (2D) numerical flow simulations are performed using the STARS simulator of Computer Modeling Group [30]. Two kinds of reservoirs are studied: a homogeneous reservoir consisting entirely of clean sand; a heterogeneous reservoir consisting of two rock types, clean sand and low-permeability mudstone. Heterogeneous realizations are generated by use of unconditional sequential indicator simulation (SIS) with the SGeMS simulator [31] developed at Stanford University.

The initial reservoir temperature and pressure are assumed to be 286.15 K and 15 bars, respectively. Bitumen considered in this research is "live," comprising of a mixture of 10.22 mol% methane (C_1) and 89.78 mol% dead Athabasca bitumen. The corresponding gas-to-oil-ratio is 5.0 m^3/m^3.

The reservoir model used is of dimensions 141 m × 500 m × 20 m in the *x*, *y*, and *z* directions, respectively, in which the y direction is along the well pair; the dimensions of this model are comparable with those used in prior simulation studies conducted at the scale of a single well pair (e.g., Jha et al. [13]). The model is discretized into 141 × 1 × 40 grid blocks in the *x*, *y*, and *z* directions, respectively. That is, each grid block is 1 m × 0.5 m in the *x*-*z* plane. In 2D flow simulations in heterogeneous reservoirs, grid blocks of dimensions 1 m × 1 m in the *x*-*z* plane are conventionally used [9,32]. In this paper, discretization along the *z*-direction is made finer to further reduce numerical dispersion. The lateral, top and bottom boundaries of the reservoir model are impermeable to fluid flow.

Both the injection and production wells are situated in the 71st grid column from the left boundary of the reservoir model. The injection and production wells are, respectively, located in the 28th and 36th grid layers from the reservoir top.

The temperature of the injected stream is equivalent to the saturation temperature of water at the operating pressure, 35 bars. The steam quality used is 90%. The production well is subject to a minimum bottom-hole pressure constraint of 15 bars, which is the initial reservoir pressure, a maximum liquid flow rate constraint of 1400 m^3/day at surface conditions, and steam trap control with a minimum subcool of 10 K. For both homogeneous and heterogeneous models, the reservoir is subject to an initial heating period of approximately 6 months using steam, following which production is commenced.

Heat losses to the over and underburden are considered in the simulations; the thermal conductivities of the overburden and underburden are set to 660 kJ/m day ° C. For simplicity, capillary pressures and asphaltene precipitation are not considered. The modeling of phase-specific relative permeabilities in this paper is based on Keshavarz et al. [1]. A summary of the reservoir model is presented in Table 1.

The levels of numerical dispersivities for the current simulation study were analyzed by following the research of Adepoju et al. [28], Garmeh [33], and Garmeh and Johns [34] along with dynamic simulation conditions for the homogeneous case and one heterogeneous realization. It was confirmed that the numerical dispersion is approximately 50% of the largest grid-block dimension, which is 0.5 m in the current reservoir model. Details of this analysis can be found in Ref. [35].

Flow velocities in the vicinity of a chamber edge in the current simulation cases are on the order of several to ten cm per day. At these velocities, numerical dispersion controls components' mixing; that is, small Fickian diffusion coefficients for solvent in bitumen (e.g., 4.32×10^{-5} m^2/day for *n*-C_6 in bitumen [26]) has no practical significance in the current simulations.

Experimental measurements of hydrodynamic dispersion coefficients for mixtures of solvent and bitumen under gravity drainage have not been published, to the best of our knowledge. Hydrodynamic dispersivity depends at least on average particle size, local heterogeneity, and flow distance [27,36,37]. Longitudinal dispersivities were reported to range from 10^{-4} m at lab scale to 100 m at field scale [28,37]. Data for transverse dispersivities are much scarcer. However, common ratios of longitudinal to transverse dispersivities are 3–30 in the literature [37,38]. A ratio of 3 was also measured by Alkindi et al. [39] in their dispersion experiment using ethanol (diluent) and glycerol, mimicking solvent dispersion in heavy oil. Then, transverse dispersivities may be estimated to range up to a few meters for typical flow distances along the edge of a steam chamber in SAGD (e.g., 10–100 m). Therefore, the numerical dispersivity estimated for the current simulation model, 0.5 m, is unlikely beyond the expected range of transverse dispersivity at SAGD's field scale.

2.2 Fluid Model. The molecular weight of the dead Athabasca bitumen used is 530 g/mol [40]. The dead bitumen has been characterized as a single pseudocomponent ("dead bitumen"

Table 1 Summary of the reservoir model used in simulation case studies

Property	Value
Initial reservoir pressure at the depth of 280 m	15 bars
Initial reservoir temperature	286.15 K
Three-phase relative permeability model (CMG, 2011-16)	Linear Interpolation
Formation compressibility	1.8×10^{-5} 1/kPa
Rock heat capacity (Keshavarz et al. [1])	2600 kJ/m^3 °C
Rock thermal conductivity (Keshavarz et al. [1])	660 kJ/m day °C
Over/underburden heat capacity (Keshavarz et al. [1])	2600 kJ/m^3 °C
Over/underburden thermal conductivity (Keshavarz et al. [1])	660 kJ/m day °C
Bitumen thermal conductivity	11.5 kJ/m day °C
Gas thermal conductivity	2.89 kJ/m day °C
Producer bottom-hole pressure (minimum)	15 bars
Steam quality	0.9

component, or C_D) using the Peng-Robinson (PR) EOS [41,42] with the characterization method of Kumar and Okuno [43]. The critical temperature, pressure, and acentric factor of C_D are 847.17 K, 10.64 bars, and 1.0406, respectively. Simulations for SAGD use three components: water, C_1, and C_D. Those for ES-SAGD use four components: water, C_1, C_D, and normal hexane (n-C_6).

Compositional behavior of water/solvent/Athabasca-bitumen mixtures is modeled using the PR EOS with van der Waals' mixing rules. The binary interaction parameter (BIP) for C_D with n-C_6 is 0.088 [40].

The BIPs for water with n-alkanes are calculated using the correlation developed by Venkatramani and Okuno [44], which is based on the three-phase curves (oleic-vapor-aqueous) of water/n-alkane binaries measured by Brunner [22]. The correlation is given as

$$\text{BIP} = c_1[1 + \exp(c_2 - c_3\text{MW})]^{-1/c_4} \quad (1)$$

where $c_1 = 0.24200$, $c_2 = 65.90912$, $c_3 = 0.18959$, and $c_4 = -56.81257$, and MW is the molecular weight of the n-alkane.

The BIP for water with C_D is estimated by reducing the BIP calculated from Eq. (1) using a scaling factor (λ) less than unity. The optimum value of λ has been determined to be 0.70 by matching the x_{wL} data measured for Athabasca bitumen by Amani et al. [20,21]. The resulting BIP for water with C_D is 0.169 [16].

The phase behavior is reflected in the simulations in terms of K values (or equilibrium constants) tabulated as functions of temperature and pressure. The K values used in the simulations with STARS are independent of composition. K values of all components corresponding to oleic-vapor-aqueous equilibrium are generated by use of the PR EOS for a fixed overall composition of 90 mol% water and 10 mol% hydrocarbons. For ES-SAGD, the overall distribution of hydrocarbons is set to 2 mol% solvent and 8 mol% live bitumen. This overall composition is considered to be representative of conditions near the chamber edge. Keshavarz et al. [1] demonstrated that the simulated cumulative bitumen production histories are little affected by the choice of overall composition to generate K values when the mixing ratio of solvent to live bitumen in the overall mixture is in the range of 0.2–0.6.

3 Simulation Case Studies

Prior simulation studies using homogeneous reservoir models presented that oil drainage along the edge of a steam chamber in successful ES-SAGD is faster and takes place at lower temperatures than that in SAGD [1,13–16]. Consequently, an ES-SAGD chamber tends to be exposed to the overlying formation rocks with a smaller area and for a shorter period for a given production volume of bitumen. Therefore, such successful ES-SAGD is expected to result in a lower SOR than conventional SAGD for a given set of reservoir and operating conditions. This section begins by reviewing the difference between SAGD and ES-SAGD with a homogeneous reservoir model in terms of SOR and chamber geometry, which forms the basis for further comparisons under heterogeneity.

Figures 1 and 2 compare SAGD (Fig. 1) and n-C_6 SAGD (Fig. 2) at 35 bars in terms of chamber shape for a given cumulative bitumen production in a homogeneous reservoir. The values assigned to the porosity, horizontal permeability, vertical permeability, and initial oil saturation for the clean sand are 0.33, 6000 mD, 4000 mD, and 0.75, respectively. Other model parameters are given in Table 1. Figure 1 shows the simulated temperature and vapor-phase saturation maps for SAGD at 456 days, at which the cumulative bitumen production is 77,487 m^3. The cumulative SOR for this cumulative bitumen production is calculated to be 4.02.

Figure 2 shows the simulated temperature and vapor-phase saturation maps for n-C_6 SAGD at 365 days from the start of operation. The injection concentration of solvent has been set to 2 mol% for this simulation. The cumulative bitumen production at this time is 76,617 m^3, and the accompanying SOR is 2.27. That is, the cumulative SOR in n-C_6 SAGD is simulated to be lower than that in SAGD by 1.75 for almost the same bitumen production volume. Figure 2(*a*) shows that temperatures in the interior of the steam chamber are comparable to the saturation temperature of water at 35 bars (515.72 K). However, temperatures along and near the chamber edge are lower.

Table 2 presents analytical estimates for the oleic-vapor-aqueous to oleic-aqueous transition temperatures corresponding to the simulated pressure and overall compositions of grid blocks along the chamber edge. Chamber-edge grid blocks were identified on the basis of the simulated vapor-phase saturation map (Fig. 2(*b*)). The accumulation of methane has a clear impact on chamber-edge temperature near the reservoir top, and accumulation of n-C_6 contributes to the reduction in chamber-edge temperature away from the reservoir top.

Despite lower chamber-edge temperatures, n-C_6 SAGD yields a higher drainage rate of bitumen along the sides of the steam chamber through enhanced oleic-phase mobility because of x_{sL}. This results in a lower cumulative SOR and alters the steam-chamber geometry by making it less laterally extensive near the reservoir top in this case. Figures 1 and 2 are given to qualitatively explain the major difference between SAGD and ES-SAGD that is often discussed in the literature on the basis of the particular set of conditions used.

However, it is uncertain how the above-mentioned aspects of ES-SAGD are affected by reservoir heterogeneity. The main question to be addressed in this section is whether the advantage of ES-SAGD over SAGD in terms of SOR is expected to be more significant under heterogeneity. This question is of primary importance because reservoir heterogeneity largely determines the geometry of a steam chamber, which in turn affects the exposure of heated zones to the overlying formation rocks.

In the subsequent subsections, simulations for SAGD and n-C_6 SAGD are conducted for the operating pressure of 35 bars and injection concentration of 2 mol% for the solvent. Two case studies (Secs. 3.1 and 3.2), each comprising of 50 stochastically

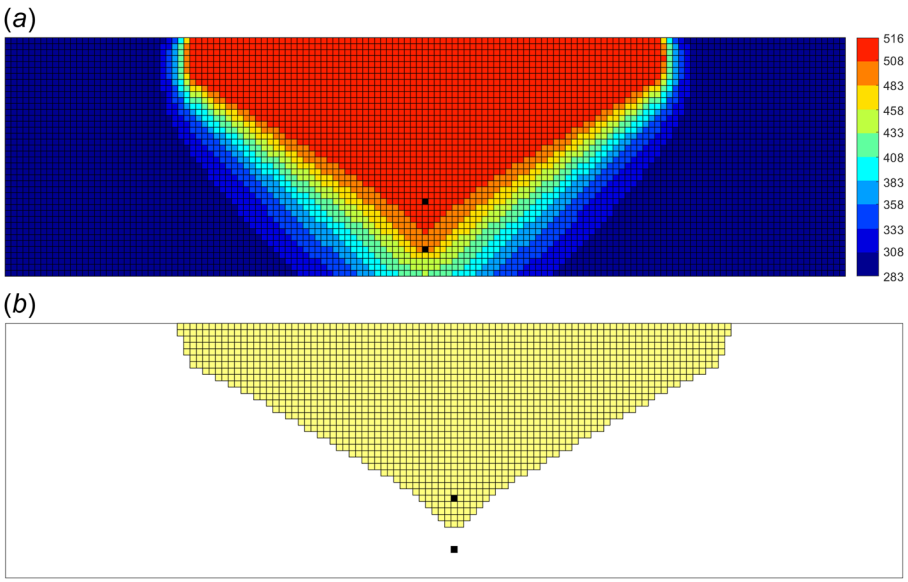

Fig. 1 Temperature (in Kelvin) and vapor-phase saturation (S_V) maps corresponding to the cumulative bitumen production of 77,487 m^3 for SAGD at 35 bars: In (*b*), S_V in grid blocks in the shaded region is greater than 5%. Injector and producer grid blocks are located in the central grid column and appear black. This cumulative bitumen production is met at 456 days.

generated heterogeneous realizations using SIS in addition to the homogeneous reservoir model, have been defined based on the orientation of simulated low-permeability mudstone barriers relative to the top and basal planes of the reservoir model, and petrophysical properties assigned to the net and non-net facies. Realizations for each case study can be viewed as equally probable vertical cross section that can be encountered by a SAGD well pair in the reservoir. Generated simulation results with realizations help obtain statistical conclusions for the two reservoir types.

For each case study, the performance of each process and reservoir is analyzed on the basis of cumulative SOR cold water equivalent as a function of cumulative bitumen production. This allows us to compare different cases on the basis of the steam usage for a given amount of bitumen production. In this paper, 2D maps for different parameters are shown for selected amounts of cumulative bitumen production, which are indicated as fractions of the simulated cumulative bitumen production in SAGD for the homogeneous model when the lateral boundaries begin to affect the propagation of the steam chamber $\left(V_{SAGD}^{hom}\right)$.

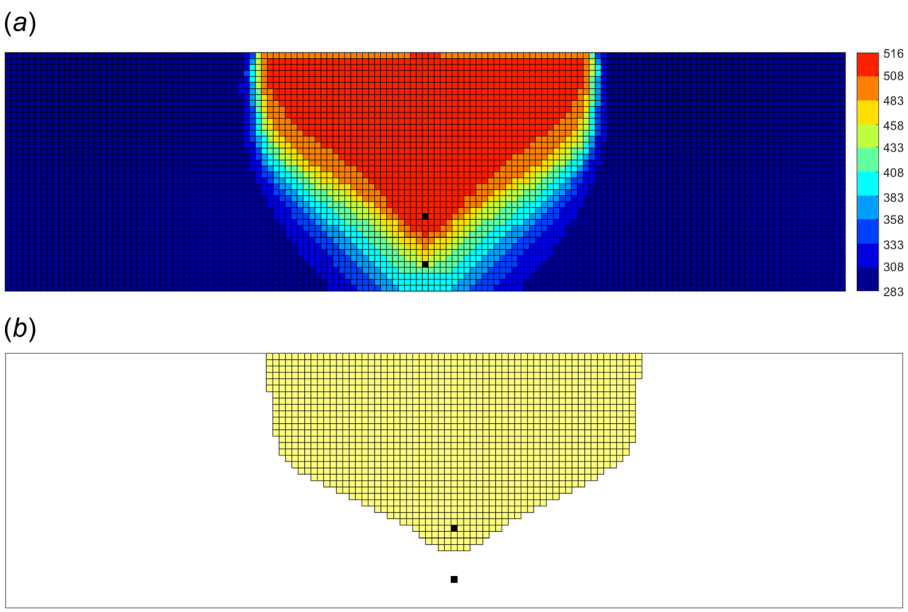

Fig. 2 Temperature (in Kelvin) and (*b*) vapor-phase saturation (S_V) maps corresponding to the cumulative bitumen production of 76,617 m^3 for *n*-C_6 SAGD at 35 bars and injection concentration of 2 mol%: In (*b*), S_V in grid blocks in the shaded region is greater than 5%. Injector and producer grid blocks located in the central grid column and appear black. This cumulative bitumen production is met at 365 days from the start of the operation.

Table 2 Analytically estimated oleic-vapor-aqueous to oleic-aqueous transition temperature ($T_{3\varphi}$) using flash calculations in n-C_6 SAGD from Fig. 2. z_i is the overall mole fraction of the ith component in a chamber-edge grid block located in a specified grid layer from the reservoir top. P is grid-block pressure. Grid blocks along the chamber edge are identified on the basis of the simulated vapor-phase saturation. Temperatures along the chamber-edge are also sensitive to z_{C1}. C_1 tends to accumulate near the reservoir top. The eighth column presents the analytical estimate of $T_{3\varphi}$ within a chamber-edge grid block when the overall composition is normalized after neglecting the presence of C_1. The ninth column presents the difference between the two estimates for $T_{3\varphi}$, showing the impact of z_{C1} on chamber-edge temperature.

Grid layer from the top	z_{C1}, mol%	z_{C6}, mol%	z_{CD}, mol%	z_w, mol%	P, bars	$T_{3\varphi}$, K	$T_{3\varphi}$, K (without C_1)	$\Delta T_{3\varphi}$, K
1	1.9415	0.1075	8.8163	89.1347	34.68	303.00	515.00	212.00
2	1.8539	0.4598	8.6933	88.9930	34.68	314.00	512.00	198.00
3	1.7091	0.0683	8.8611	89.3615	34.69	322.00	514.25	192.25
4	1.6824	0.0467	8.8751	89.3958	34.70	325.00	514.25	189.25
5	2.1944	16.5461	3.3617	77.8978	34.71	418.00	476.00	58.00
6	1.8579	7.9512	6.6064	83.5844	34.75	396.00	485.00	89.00
7	1.5210	1.4973	8.5556	88.4261	34.79	369.00	507.00	138.00
8	1.4563	0.1633	8.9337	89.4468	34.79	358.00	513.75	155.75
9	1.2145	0.0156	9.0098	89.7601	34.79	405.00	514.55	109.55
10	1.0320	0.0032	9.0377	89.9271	34.78	440.00	514.60	74.60
11	0.9866	0.0017	9.0364	89.9753	34.77	447.00	514.60	67.60
12	0.9829	0.0013	9.0287	89.9870	34.77	447.00	514.60	67.60
13	0.9852	0.0012	9.0231	89.9906	34.78	447.00	514.60	67.60
14	0.9882	0.0013	9.0207	89.9898	34.78	446.00	514.60	68.60
15	1.3857	11.7017	1.0975	85.8151	34.75	423.00	475.00	52.00
16	0.8509	1.7591	5.9557	91.4343	34.79	425.00	502.00	77.00
17	0.8069	9.7422	0.7158	88.7351	34.75	443.00	474.00	31.00
18	0.7557	9.2874	0.9725	88.9844	34.76	444.00	475.00	31.00
19	0.8546	11.0159	1.0501	87.0795	34.75	446.00	475.00	29.00
20	0.7236	11.2886	0.9398	87.0481	34.77	452.00	475.00	23.00
21	0.7143	12.3100	1.0853	85.8904	34.78	455.00	475.00	20.00
22	0.6039	13.0000	1.3061	85.0900	34.79	459.00	475.00	16.00
23	0.4916	12.6068	1.6201	85.2815	34.80	462.00	475.00	13.00
24	0.3623	11.6884	1.8751	86.0742	34.81	466.00	476.00	10.00
25	0.2652	10.8395	2.0480	86.8473	34.82	468.00	476.00	8.00
26	0.1802	9.9731	2.1805	87.6662	34.83	471.00	476.00	5.00
27	0.0978	8.7038	2.3920	88.8065	34.85	473.00	477.00	4.00
28	0.1468	8.8432	2.5242	88.4859	34.88	472.00	477.00	5.00
29	0.0628	6.6407	2.9201	90.3764	34.90	476.00	479.00	3.00
30	0.0750	6.7824	3.0205	90.1222	34.93	476.00	479.00	3.00
31	0.0199	3.5293	3.3330	93.1178	34.95	485.00	487.00	2.00

3.1 Case Study 1: Horizontal Mudstone Barriers. In this case study, the orientation of the simulated mudstone barriers is horizontal. Table 3 summarizes the pertinent parameters used to generate the realizations using SIS. The values assigned to porosity, horizontal permeability, vertical permeability, and initial oil saturation for the clean sand are 0.33, 6000 mD, 4000 mD, and 0.75, respectively. The corresponding values for the mudstone facies are set to 0.02, 6000 mD and 0.04 mD, and 0.15. The reservoir models and the assignment of facies properties in this case study are consistent with the conventional approach used in reservoir engineering studies focusing on effects of mudstone barriers on SAGD performance (e.g., Chen et al. [7]; Wang and Leung [9]). In this modeling paradigm, mud layers within a given muddy flow simulation grid block are assumed to be thin such that their influence on the hydraulic conductivity of the grid block is restricted only to its vertical permeability.

The simulated value of V_{SAGD}^{hom} in this case study is approximately 196,190 m^3; the corresponding recovery factor is 64%. Tables 4 and 5 compare the cumulative SOR for SAGD and n-C_6 SAGD across different realizations for the cumulative bitumen productions of 49,048 m^3 ($0.25V_{SAGD}^{hom}$) and 98,095 m^3 ($0.50V_{SAGD}^{hom}$), respectively. The realizations in these tables are labeled using numerical indices; the homogeneous case has been assigned the index of zero. Note that these cumulative bitumen production targets are not met by all realizations, which leads to gaps in these tables. This is either due to the presence of mudstone distributions that severely impede the propagation of the steam chamber within the reservoir, or nonconvergence of numerical solution. The latter issue was observed to be prevalent with n-C_6 SAGD and is likely due to reservoir models exhibiting extreme contrasts in permeability over short length scales. Nevertheless, the realizations depicted in Tables 4 and 5 qualitatively exhibit a wide variety of steam chamber geometry.

Tables 4 and 5 show the cumulative SORs for a fixed cumulative bitumen production to be systematically lower under steam-solvent coinjection relative to steam-only injection. For each cumulative bitumen production, a paired t-test on the two sets of SORs was performed to verify that the difference in SOR between SAGD and n-C_6 SAGD for a specified cumulative bitumen production is statistically significant. As described for a specific case below, reduction of the cumulative SOR under steam-solvent coinjection is attributed to the combination of improved oleic-phase mobility due to x_{sL} and lower thermal losses to the overburden, although relative magnitudes of contribution from different factors depend on the reservoir heterogeneity under consideration.

Table 3 Input parameters for SIS for heterogeneous reservoir models comprising of clean sand and mudstone for the first case study in Sec. 3 (see Sec. 3.1). The spherical model is used for the indicator variogram for the mudstone facies.

Property	Value
Global proportion of clean sand	0.75
Global proportion of mudstone	0.25
Nugget effect for indicator variogram model	0.10
Azimuth for variogram model	90 deg
Horizontal range parameter, m	25.0
Vertical range parameter, m	1.0

As with the homogeneous case, steam-solvent coinjection can reduce heat losses to the overburden in heterogeneous reservoirs by the reduction of operating chamber temperatures and exposed area for heat transfer. This is illustrated in Fig. 3, which presents the simulated vapor-phase saturation and temperature maps for SAGD and n-C_6 SAGD for realization 23 for a cumulative bitumen production of approximately 98,095 m^3. The diminished lateral span of the steam chamber near the top for n-C_6 SAGD comes from the reduction of the oleic-vapor-aqueous to oleic-aqueous transition temperature at the chamber edge due to the accumulation of n-C_6. For this realization, Figs. 4 and 5, respectively give the cumulative water injected and cumulative heat losses as a function of cumulative bitumen production for each process.

The extent to which each process is detrimentally affected by heterogeneity is quantified in terms of the resulting increase in cumulative SOR for a given cumulative bitumen production. That is, the metric $(SOR_{het} - SOR_{hom})$ is evaluated for each process and realization as a function of cumulative bitumen production. The terms, SOR_{het} and SOR_{hom}, represent the cumulative SORs for a given heterogeneous realization and homogenous reservoir, respectively. The adverse effect of reservoir heterogeneity on a given process diminishes with decreasing values of this metric.

Tables 4 and 5 also present the values of $(SOR_{het} - SOR_{hom})$ for SAGD and n-C_6 SAGD across different realizations for the cumulative bitumen productions of 49,048 and 98,095 m^3, respectively. For the cumulative bitumen production of 49,048 m^3, SAGD yields an average value of 3.61 for $(SOR_{het} - SOR_{hom})$, while n-C_6 SAGD yields the value of 2.37 for the same; the corresponding variances are 4.99 and 1.92. For the cumulative bitumen production of 98,095 m^3, pertinent means are 3.11 and 1.94, and the respective variances are 1.23 and 0.51. Hence, n-C_6 SAGD, on average, is adversely affected by heterogeneity to a lesser extent compared to SAGD for these simple cases. A paired t-test was conducted for the two sets of values for $(SOR_{het} - SOR_{hom})$ for each cumulative bitumen production to ensure that the above conclusion is statistically valid.

The reduction in cumulative SOR due to coinjection for a given realization is calculated as $(SOR_{SAGD} - SOR_{ES-SAGD})$ as a

Table 4 Cumulative SOR for SAGD and n-C_6 SAGD for a cumulative bitumen production of 49,048 m^3 for realizations in case study Sec. 3.1. The homogeneous reservoir model is denoted as "realization 0." The average increase in SOR due to heterogeneity (Δ_{het}SOR) for SAGD is 3.61; the corresponding value for n-C_6 SAGD is 2.37. The average reduction in SOR due to coinjection of solvent (Δ_{sol}SOR) for the heterogeneous cases is 2.51.

Realization	Time, days (SAGD)	Time, days (n-C_6 SAGD)	SOR (SAGD)	SOR (n-C_6 SAGD)	Δ_{het}SOR (SAGD)	Δ_{het}SOR (n-C_6 SAGD)	Δ_{sol}SOR
0	335.64	292.69	3.48	2.21	0.00	0.00	1.27
1	587.31	374.47	6.28	3.83	2.80	1.62	2.45
2	406.29	311.24	4.45	2.72	0.97	0.50	1.73
3	2456.75	1660.37	12.09	7.89	8.61	5.67	4.21
4	711.49	463.98	6.28	4.12	2.79	1.91	2.15
5	845.02	535.97	6.71	4.38	3.23	2.17	2.33
6	972.83	569.00	7.65	5.28	4.17	3.07	2.37
8	395.16	312.13	4.17	2.68	0.69	0.47	1.48
9	1426.60	1202.36	5.56	3.34	2.08	1.13	2.22
10	1229.49	1292.82	5.44	3.48	1.95	1.27	1.95
12	758.01	456.37	6.65	4.06	3.17	1.85	2.59
13	816.92	485.81	7.07	4.18	3.59	1.96	2.90
14	1073.40	577.43	7.03	4.79	3.54	2.58	2.23
15	455.63	327.95	4.42	2.91	0.94	0.70	1.51
16	1957.39	997.11	12.71	7.50	9.23	5.28	5.21
17	1504.20	907.47	9.54	6.87	6.06	4.65	2.68
18	771.01	524.90	6.38	4.13	2.90	1.92	2.25
19	3077.38	2986.34	8.50	4.37	5.02	2.16	4.13
20	916.43	607.57	7.05	5.02	3.56	2.81	2.02
21	779.47	503.36	6.62	4.43	3.13	2.21	2.19
22	1746.62	776.65	11.27	6.25	7.79	4.04	5.02
23	957.53	632.26	6.31	4.91	2.82	2.70	1.39
24	713.62	438.37	6.64	4.13	3.15	1.91	2.51
25	556.41	407.32	5.26	3.77	1.78	1.56	1.49
27	434.33	313.13	4.48	2.74	0.99	0.53	1.73
28	528.93	351.31	5.12	3.21	1.63	0.99	1.91
29	1189.98	660.44	8.91	4.98	5.43	2.77	3.93
30	607.19	443.62	5.91	4.27	2.43	2.06	1.64
31	460.66	324.35	4.97	2.94	1.48	0.73	2.02
32	665.92	426.38	6.34	4.07	2.86	1.85	2.28
33	968.80	653.16	7.55	5.67	4.06	3.45	1.88
35	452.36	351.36	4.54	3.50	1.05	1.29	1.03
36	563.17	375.76	5.26	3.63	1.78	1.41	1.63
37	2536.65	1314.84	10.05	7.27	6.57	5.06	2.78
38	506.14	390.32	4.72	3.09	1.24	0.88	1.63
39	3435.87	1334.58	12.40	7.39	8.91	5.17	5.01
40	423.88	315.80	4.30	2.76	0.82	0.55	1.54
41	1493.59	1484.47	5.85	3.91	2.37	1.70	1.94
42	938.25	576.35	7.34	5.27	3.86	3.06	2.07
43	1632.89	1703.93	8.57	5.17	5.08	2.96	3.39
44	922.14	546.72	7.55	5.31	4.06	3.09	2.24
45	1882.66	2186.61	6.72	4.06	3.24	1.85	2.66
47	2499.51	1090.16	10.68	6.77	7.20	4.55	3.91
48	805.83	465.73	8.04	4.74	4.56	2.53	3.30
49	587.77	392.15	5.91	4.08	2.43	1.87	1.83
50	1485.66	866.68	9.88	6.48	6.40	4.27	3.40

Table 5 Cumulative SOR for SAGD and n-C_6 SAGD for a cumulative bitumen production of 98,095 m^3 for realizations in case study sec. 3.1. The homogeneous reservoir model is denoted as "realization 0." The average increase in SOR due to heterogeneity (Δ_{het}SOR) for SAGD is 3.11; the corresponding value for n-C_6 SAGD is 1.94. The average reduction in SOR due to coinjection of solvent (Δ_{sol}SOR) for the heterogeneous cases is 2.75.

Realization	Time, days (SAGD)	Time, days (n-C_6 SAGD)	SOR (SAGD)	SOR (n-C_6 SAGD)	Δ_{het}SOR (SAGD)	Δ_{het}SOR (n-C_6 SAGD)	Δ_{sol}SOR
0	526.68	425.06	3.92	2.34	0.00	0.00	1.58
2	788.33	483.24	5.39	3.11	1.47	0.77	2.28
4	1632.45	794.23	7.49	4.32	3.57	1.97	3.18
5	1444.91	846.16	6.87	4.68	2.95	2.34	2.19
6	1768.28	865.30	7.84	4.82	3.92	2.47	3.02
8	1064.01	581.24	6.09	3.72	2.17	1.38	2.37
9	1937.70	1424.33	6.04	3.61	2.12	1.27	2.43
10	1734.44	1493.89	6.02	3.44	2.10	1.10	2.57
12	1678.14	774.70	7.63	4.11	3.71	1.77	3.52
13	1745.29	786.39	8.06	4.06	4.14	1.72	4.00
14	1772.76	838.46	7.19	4.44	3.26	2.10	2.74
15	1174.30	598.35	6.27	3.91	2.35	1.57	2.35
17	2430.06	1426.48	8.42	6.25	4.50	3.91	2.16
18	1557.55	782.38	7.43	3.99	3.51	1.65	3.44
20	1371.69	793.54	6.72	4.22	2.80	1.88	2.50
21	1528.50	763.71	7.36	4.23	3.44	1.89	3.13
23	3526.86	1300.45	9.77	5.62	5.85	3.28	4.15
25	1533.90	685.37	8.20	4.54	4.28	2.20	3.66
27	977.87	505.88	5.95	3.29	2.03	0.95	2.66
28	1456.76	686.52	6.92	4.32	3.00	1.98	2.60
30	1608.53	797.56	8.11	4.94	4.19	2.59	3.17
31	1026.15	565.03	6.07	3.90	2.15	1.55	2.18
32	1441.23	697.33	7.64	4.59	3.72	2.25	3.05
35	1239.99	703.34	6.62	4.65	2.70	2.30	1.97
36	1065.39	564.65	6.06	3.73	2.14	1.38	2.34
38	843.83	552.38	5.08	3.14	1.16	0.79	1.94
40	1105.25	591.25	6.35	3.82	2.43	1.48	2.53
41	1859.34	1695.61	5.82	3.94	1.90	1.60	1.89
42	1781.57	875.91	7.28	4.27	3.36	1.92	3.02
43	2563.51	2039.50	8.74	5.20	4.82	2.85	3.54
45	2106.50	2390.88	5.32	4.03	1.40	1.68	1.29
49	1300.40	691.17	7.38	4.47	3.46	2.13	2.91
50	2184.12	1146.28	8.83	5.73	4.91	3.39	3.10

function of cumulative bitumen production; the terms SOR_{SAGD} and $SOR_{ES\text{-}SAGD}$, respectively, represent cumulative SORs for SAGD and ES-SAGD for a given cumulative bitumen production. Tables 4 and 5 also present the variation of this metric across different realizations for the cumulative bitumen productions of 49,048 and 98,095 m^3, respectively.

For the heterogeneous cases, the average value of $(SOR_{SAGD} - SOR_{ES-SAGD})$ is 2.51 for the cumulative bitumen productions of 49,048 m^3, and 2.75 for the cumulative bitumen production of 98,095 m^3; the corresponding values for the homogeneous case (realization 0) are 1.27 and 1.58. That is, on average, the reduction in cumulative SOR due to coinjection of solvent is simulated to be greater for the heterogeneous cases compared to the homogeneous case (realization 0). This is influenced by two factors. First, the extent to which the time taken to meet a given cumulative bitumen production is reduced due to steam-solvent coinjection is on average greater under heterogeneity (e.g., see Table 5). Second, the reduction in cumulative SOR due to the accelerated lateral expansion of the steam chamber is offset to a lesser extent by thermal losses to the overburden due to a smaller exposed area under reservoir heterogeneity (see Fig. 3, as an example).

In heterogeneous reservoirs, the amount of solvent-diluted oil is expected to be higher than that under homogeneity. This is because more tortuous hydraulic paths in a heterogeneous reservoir not only facilitates the mixing of solvent with mobile bitumen (i.e., dispersive flux in the transverse direction along the edge of a steam chamber), but also increases the retention time for the injected solvent in the reservoir. That is, the ratio of dispersive flux in the transverse direction to convective flux in the longitudinal direction along the chamber edge tends to be increased under heterogeneity. This can be viewed to be analogous to the well-known situation of gas injection in which the mixing of gas components with bypassed oil in a heterogeneous reservoir is enhanced when Damköhler number is increased in convection-dispersion-capacitance behavior of oil displacement by gas [45–47]. The questions to be answered below are whether and to what extent x_{sL} is enhanced under heterogeneity.

Table 6 presents the ratio of the accumulated solvent volume to the cumulative bitumen production (i.e., solvent retention ratio) for the homogeneous and heterogeneous models in the current case study for a cumulative bitumen production of 98,095 m^3 ($0.50V_{SAGD}^{hom}$). Table 6 clearly indicates that the retained volume of solvent for a given cumulative bitumen production increases under heterogeneity. Details of the simulation have indicated that the increase in solvent accumulation is sensitive to the spatial distribution of mudstone barriers.

Simulations for some realizations exhibit that the liquid solvent accumulates in regions with low oleic-phase mobility, or above laterally extensive mudstone bodies located near the well pair. For example, let us consider realization 23 in this case study (see Fig. 3). Figure 6(*a*) presents the simulated x_{sL} distribution map for a cumulative bitumen production of approximately 98,095 m^3 for this realization, and Fig. 7(*a*) presents the corresponding map for the homogeneous case. The areal span of regions of elevated x_{sL} (>80 mol%) is greater for the heterogeneous cases compared to that observed for the homogeneous case depicted in Fig. 7(*a*). As presented in the maps for the oleic-phase mole fraction (β_L) (Fig. 6(*b*)) and the product of β_L and x_{sL} (Fig. 6(*c*)), however, the relative mobility of the oleic phase within the clean sand grid blocks whose x_{sL} values are elevated can be quite low. Even when the

oleic-phase saturation in these grid blocks is high enough for the oleic phase to be mobile (e.g., near the top of the model in Fig. 6(*d*)), such regions are often situated above laterally extensive mudstone barriers, which impede the drainage of the oleic phase toward the production well. Discrepancies in the distribution of x_{sL} between the homogeneous and heterogeneous cases are interdependent with the differences in the corresponding temperature distributions (this is also true for case study 2). This is apparent from comparison of the temperature map given in Fig. 7(*b*) for the homogeneous case and Fig. 3(*d*) for realization 23 for the cumulative bitumen production of approximately 98,095 m^3.

To recap on the main point from this case study, the advantage of n-C_6 SAGD over SAGD in terms of SOR was simulated to be more significant under heterogeneity with horizontal mudstone bodies. The mechanisms exemplified for a homogeneous reservoir in Figs. 1 and 2 were enhanced mainly because of a larger amount of solvent residing in the oleic phase under heterogeneity. Distributions of temperature and the dissolution of solvent in the oleic phase near the chamber edge are connected phenomena through the interplay between phase behavior and flow under heterogeneity. At a given time and location within the reservoir, temperature dictates the extent to which the solvent dissolves in the oleic phase near the chamber edge. x_{sL} near the chamber edge determines the volatility of the oleic phase and hence, influences the extent to which the solvent is vaporized upon subsequent contact with steam; this affects the extent to which the solvent accumulates near the chamber edge, and consequently, the temperature distribution along it. The temperature distribution near the chamber edge in turn influences the geometry of a steam chamber and the cumulative SOR. These arguments reinforce the importance of

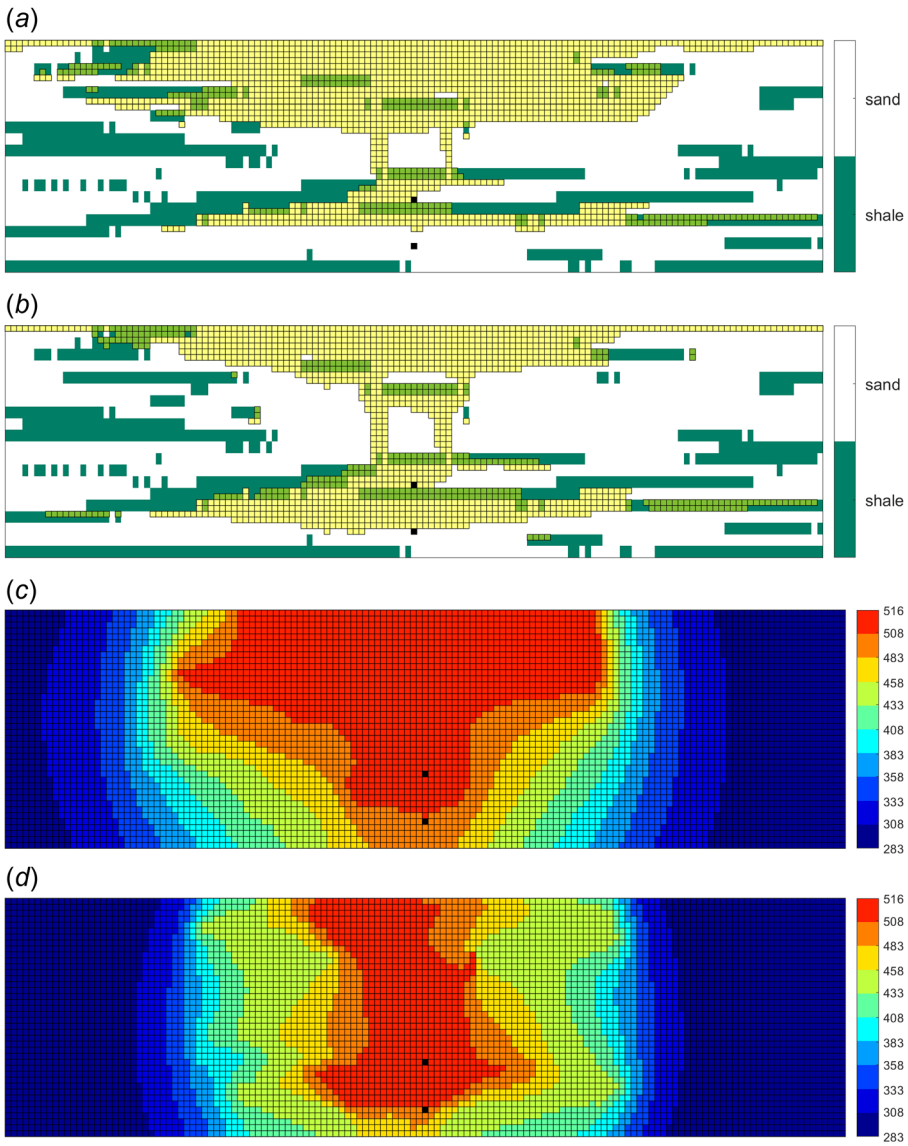

Fig. 3 Vapor-phase saturation (S_v) and temperature (in Kelvin) maps for SAGD and *n*-C_6 SAGD for realization 23 at the cumulative bitumen production of approximately 98,095 m^3 ($0.50V_{SAGD}^{hom}$): (*a*) S_v map for SAGD, (*b*) S_v map for *n*-C_6 SAGD, (*c*) temperature map for SAGD, and (*d*) temperature map for *n*-C_6 SAGD. In part (*a*), the grid blocks in the lightly-shaded region correspond to S_v-values greater than 5%. Injector and producer grid blocks are located in the central grid column and appear black. Near the well pair, the chamber for ES-SAGD is larger than that of SAGD while the opposite is true toward the top of the model. The aforementioned cumulative bitumen production is reached at 3527 days for SAGD and at 1300 days for *n*-C_6 SAGD; this includes the initial heating period of 183 days (also see Table 5).

mixing between bitumen and solvent near the chamber edge, and its understanding for effective implementation of ES-SAGD under heterogeneity.

3.2 Case Study 2: Inclined Mudstone Barriers. In this section, the applicability of the conclusions regarding the relative performance of *n*-C_6 SAGD to SAGD obtained using the reservoir models in Sec. 3.1 is examined for those more representative of the middle McMurray member.

As with Sec. 3.1, the relative performance of ES-SAGD to SAGD is evaluated by use of a two-facies reservoir model comprising of clean sand and mudstone with unconditional SIS in this section. The reservoir gridding is identical to that described in Sec. 2.1. The dimensions of the grid cells used for geostatistical modeling are identical to that used in flow simulation; that is, neither upscaling nor grid refinement is performed. The assignment of petrophysical properties of clean sand and mudstone is informed by experimental data reported by Musial et al. [48]. The porosity, horizontal and vertical permeabilities, and bitumen saturation of the clean sand facies have been set to 36%, 6100 mD and 3500 mD, and 85%, respectively. The corresponding values for mudstone facies are 5%, 1 mD and 0.1 mD, and 15%. So, a major distinction between the heterogeneous models used in this case study and those used previously is the spatial discontinuity of the horizontal component of the hydraulic conductivity (i.e., k_x). The values for the reservoir properties assigned to the non-net facies in these simulations are identical to those reported by Musial et al. [48] for clay plugs, which exhibit the poorest petrophysical characteristics among the five facies associations studied by the authors. This facilitates the obtainment of conservative estimates for the production performance of SAGD and n-C_6 SAGD. Table 7 presents values for input parameters for SIS in this case study. The predicted distributions of mudstone are inclined relative to the base and top planes of the reservoir model.

As with the first simulation case study, the extent to which reservoir heterogeneity detrimentally affects the cumulative SOR for a given cumulative bitumen production for the current case study is lower for n-C_6 SAGD compared to SAGD. Similarly, the advantage of ES-SAGD in terms of its ability to lower the consumption of steam to meet a given cumulative bitumen production

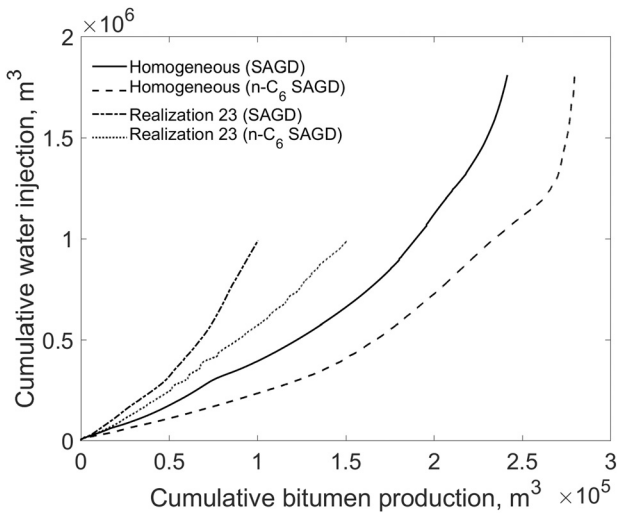

Fig. 4 Cumulative water injection as a function of cumulative bitumen production in SAGD and *n*-C_6 SAGD for the homogeneous reservoir model and realization 23 in the first case study (Sec. 3.1)

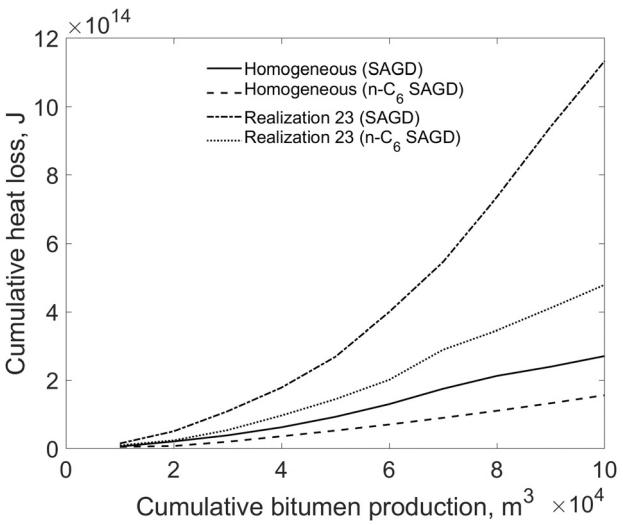

Fig. 5 Cumulative heat loss as a function of cumulative bitumen production in SAGD and *n*-C_6 SAGD for the homogeneous reservoir model and realization 23 in the first case study (Sec. 3.1)

Table 6 Solvent retention ratios for the homogeneous and heterogeneous models in the first case study (horizontal mudstone barriers) for the cumulative bitumen production of 98,095 m^3 ($0.50V_{SAGD}^{hom}$). These ratios are calculated on the basis of the simulated cumulative bitumen production, solvent injection and production histories at stock-tank conditions.

Realization	Time, days	Accumulated solvent volume, m^3	Solvent retention ratio
0 (homogeneous)	425.06	7125.10	0.07
2	483.24	14417.25	0.15
3	1932.19	11629.75	0.12
4	794.23	18727.17	0.19
5	846.16	12749.83	0.13
6	865.30	15019.29	0.15
8	581.24	13149.04	0.13
9	1424.33	13798.34	0.14
10	1493.89	13170.84	0.13
12	774.70	29721.11	0.30
13	786.39	27764.81	0.28
14	838.46	22725.20	0.23
15	598.35	10879.02	0.11
16	1651.02	30133.92	0.31
17	1426.48	29718.04	0.30
18	782.38	23640.68	0.24
19	3411.86	28892.36	0.29
20	793.54	14920.84	0.15
21	763.71	20016.15	0.20
23	1300.45	29880.59	0.30
25	685.37	14939.90	0.15
27	505.88	14187.38	0.14
28	686.52	16226.81	0.17
30	797.56	14254.97	0.15
31	565.03	9011.96	0.09
32	697.33	15576.50	0.16
34	1622.19	14001.65	0.14
35	703.34	13394.94	0.14
36	564.65	11335.42	0.12
37	1917.13	12706.92	0.13
38	552.38	13112.65	0.13
40	591.25	16418.41	0.17
41	1695.61	11725.57	0.12
42	875.91	18797.29	0.19
43	2039.50	27323.69	0.28
45	2390.88	12939.54	0.13
47	1967.40	46006.40	0.47
49	691.17	22802.83	0.23
50	1146.28	18096.80	0.18

is more pronounced when mudstone barriers spatially conform to moderately impede the vertical propagation of the steam chamber.

The value of V_{SAGD}^{hom} is 218,795 m^3 for the current case study. Table 8 captures the variation in cumulative SOR across different realizations for a cumulative bitumen production of 54,699 m^3 ($0.25V_{SAGD}^{hom}$); Table 9 presents the same for a cumulative bitumen production of 98,458 m^3 ($0.45V_{SAGD}^{hom}$). These tables also present pertinent values for the reduction in cumulative SOR due to coinjection of solvent for the aforementioned cumulative bitumen productions.

The combination of improved drainage rate due to x_{sL}, and lower heat losses to the overburden due to lower temperatures and exposed area of transfer results in lower cumulative SORs in steam-solvent coinjection compared to steam-only injection for the current case study. This is shown in Figs. 8 and 9, which, respectively, present the vapor-phase saturation and temperature maps for realization 17 for the cumulative bitumen production of approximately 98,458 m^3. Figures 10 and 11, respectively, give the variation in cumulative water injected and cumulative heat loss as a function of cumulative bitumen production for this realization.

Further, it is also observed that in situ retention of solvent for a given cumulative bitumen production is greater for the heterogeneous reservoirs considered in this case study relative to the homogeneous case. Table 10 presents the solvent retention ratios for different realizations for the cumulative bitumen production of

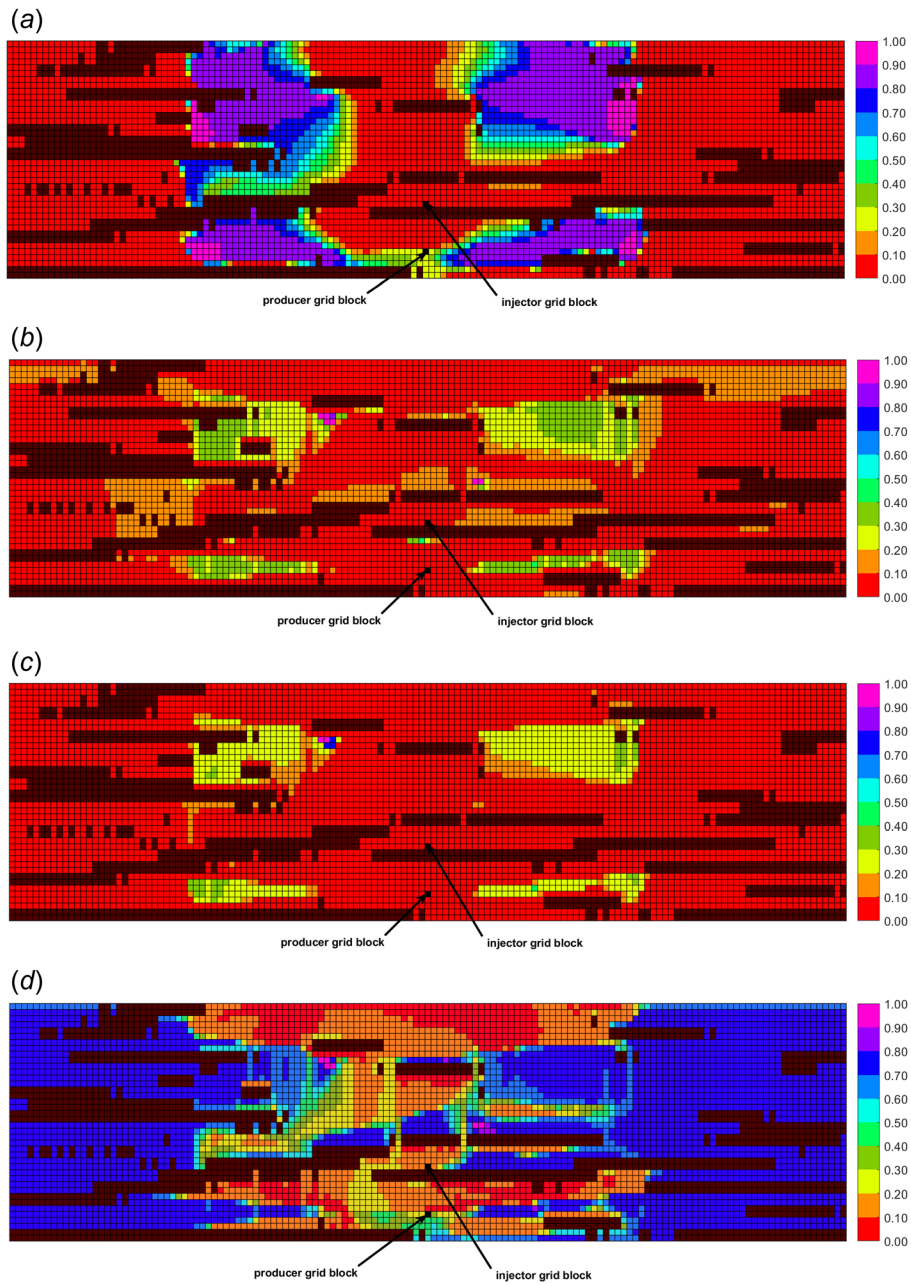

Fig. 6 Property maps for clean sand grid blocks in n-C_6 SAGD for realization 23 from the first case study for the cumulative bitumen production of 98,095 m^3 ($0.50V_{SAGD}^{hom}$): (*a*) x_{sL} map, (*b*) β_L map, (*c*) $\beta_L x_{sL}$ map, and (*d*) S_L map. Mudstone barriers are indicated in the background. This cumulative bitumen production is met at 1300 days from the start of the operation.

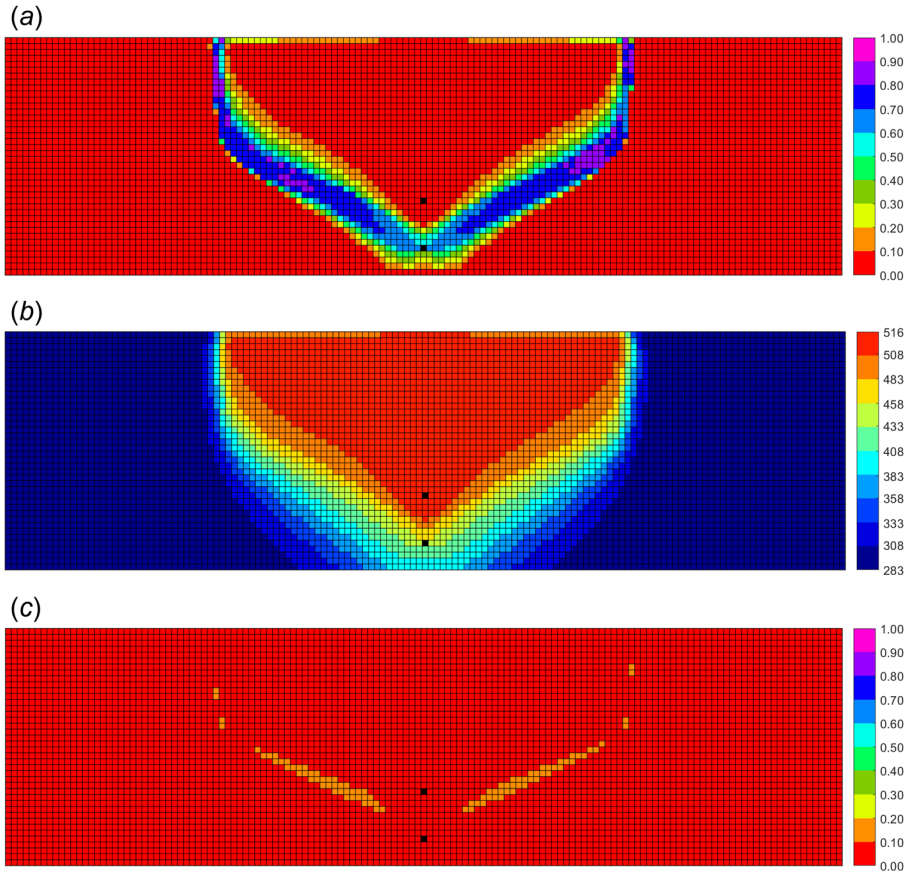

Fig. 7 x_{sL}, temperature and $\beta_L x_{sL}$ maps in n-C_6 SAGD for the homogeneous model in the first case study for the cumulative bitumen production of approximately 98,095 m^3 ($0.50V_{SAGD}^{hom}$): (*a*) x_{sL} map, (*b*) temperature map, and (*c*) $\beta_L x_{sL}$ map. Injector and producer grid blocks are located in the central grid column and appear black. This cumulative bitumen production is met at 425 days from the start of the operation.

98,458 m^3. The advantage of n-C_6 SAGD over SAGD that is simulated to be enhanced under heterogeneity can be explained by the larger amount of solvent being used for a given bitumen production under heterogeneity than homogeneity. However, the excess retention of solvent is not necessarily desirable considering that a fraction of the solvent is unlikely recoverable.

Figure 12 presents maps for x_{sL}, oleic-phase saturation, mole fraction of the oleic phase (β_L), and the product of β_L and x_{sL} for the clean sand grid blocks in realization 17 of this case study for the cumulative bitumen production of approximately 98,458 m^3. The x_{sL} maps for realization 23 from the previous case study (Fig. 6) and realization 17 from this case study (Fig. 12(*a*)) indicate that under certain reservoir architectures, significant solvent–bitumen mixing can occur in immobile regions near the reservoir top.

An approach to reducing solvent accumulation within the reservoir over a long term is to adopt a time-variant injection concentration strategy (VC) using a condensable solvent, wherein the injection concentration of the solvent is gradually reduced and culminates in steam-only injection [14]. In heterogeneous reservoirs, the optimal sequence of injection concentrations under the VC strategy is expected to be sensitive to the spatial distribution of mudstone barriers. Although not shown in this paper, Venkatramani [35] presented how excessive accumulation of solvent later in the production phase can be mitigated by use of the VC strategy for realization 17 of this case study.

A major distinction between the two case studies in terms of the observed geometry of a steam chamber is that the steam chambers for several realizations in the current case study exhibit preferential growth toward the top of the reservoir model along the direction of inclination of the mudstone barriers (see Fig. 8). This can render the steam chamber to grow asymmetrically relative to the grid column containing the well pair near the top of the model for a significant duration of the production phase. A consequence of this difference in chamber growth is that the average SOR in SAGD for a given cumulative bitumen production is greater in reservoirs with inclined mudstone bodies later in the production phase. The average reduction in the cumulative SOR due to coinjection for a given cumulative bitumen production is also observed to be higher even for lower cumulative bitumen productions. For instance, for the cumulative bitumen production of 54,699 m^3 (i.e., $0.25V_{SAGD}^{hom}$ for the second case study), the

Table 7 Input parameters for SIS for simple heterogeneous reservoir models comprising of clean sand and mudstone for the second case study (inclined mudstone barriers) in Sec. 3 (see Sec. 3.2). The spherical model is used for the indicator variogram for the mudstone facies.

Property	Value
Global proportion of clean sand	0.75
Global proportion of mudstone	0.25
Nugget effect for indicator variogram model	0
Azimuth for variogram model	78 deg
Horizontal range parameter, m	12.0
Vertical range parameter, m	1.0

Table 8 Cumulative SOR for SAGD and n-C_6 SAGD for the cumulative bitumen production of 54,699 m^3 for realizations in the second case study (Sec. 3.2). The homogeneous reservoir model is denoted as realization 0. The average increase in SOR due to heterogeneity (Δ_{het}SOR) for SAGD is 3.90; the corresponding value for n-C_6 SAGD is 2.27. The average reduction in SOR due to coinjection of solvent (Δ_{sol}SOR) for the heterogeneous cases is 2.71.

Realization	Time, days (SAGD)	Time, days (n-C_6 SAGD)	SOR (SAGD)	SOR (n-C_6 SAGD)	Δ_{het}SOR (SAGD)	Δ_{het}SOR (n-C_6 SAGD)	Δ_{sol}SOR
0	342.72	295.91	3.08	2.00	0.00	0.00	1.08
4	1238.31	598.17	7.13	3.94	4.05	1.94	3.19
6	733.95	481.50	5.22	3.56	2.14	1.56	1.66
7	778.54	501.29	6.11	4.11	3.03	2.11	2.00
12	1145.16	615.01	7.19	4.04	4.11	2.04	3.15
13	1055.56	567.87	6.55	3.64	3.46	1.64	2.90
14	1679.46	1504.71	7.51	5.19	4.43	3.20	2.32
15	562.39	372.45	4.73	2.99	1.65	0.99	1.74
16	2230.84	1080.11	12.54	7.61	9.45	5.61	4.93
17	946.46	509.93	6.82	3.63	3.74	1.64	3.19
18	930.28	541.44	6.58	4.05	3.50	2.05	2.53
20	925.78	556.06	6.30	3.95	3.22	1.95	2.35
21	648.45	405.52	4.94	3.09	1.86	1.09	1.85
23	1627.46	669.96	9.33	4.69	6.24	2.69	4.64
26	944.46	550.78	6.53	4.03	3.45	2.03	2.50
31	979.04	572.08	6.29	4.20	3.20	2.20	2.09
32	724.64	435.96	5.63	3.40	2.55	1.41	2.23
33	984.92	530.81	6.02	3.75	2.93	1.75	2.27
35	706.17	441.40	5.28	3.41	2.20	1.41	1.87
36	1557.68	811.94	8.90	5.21	5.82	3.21	3.70
37	1880.82	988.69	10.74	7.35	7.66	5.35	3.39
44	690.75	430.81	5.30	3.43	2.22	1.43	1.87
48	1337.70	702.79	7.62	4.33	4.53	2.34	3.28
49	956.29	509.77	6.59	3.68	3.51	1.68	2.91
50	1203.40	698.37	7.65	5.11	4.57	3.11	2.54

average SORs for SAGD and ES-SAGD are 7.08 and 4.57 in the first case study, and 6.98 and 4.27 in the second case study. The pertinent values for the cumulative bitumen production of 76578 m^3 are 7.35 and 4.59 in the first case study, and 7.83 and 4.62 in the second case study. The corresponding values for the cumulative bitumen production of 109398 m^3 in the first and second case studies are 7.28 and 4.38, and 8.18 and 4.59, respectively.

The current and previous simulation case studies demonstrated that SOR reduction by steam-solvent coinjection can be greater under heterogeneity than that under homogeneity. The improvement in SOR reduction under heterogeneity was shown to be a consequence of enhanced solvent/bitumen mixing and its interplay with temperature. This was also confirmed with the reservoir gridding eight times finer than the current case [35]. The performance of SAGD and ES-SAGD can be detrimentally affected in reservoirs overlain by aquifers and gas zones [9,49]. Although beyond the scope of this research, the simulation study by Zhou et al. [49] recommends the injection of a polymer into overlying aquifers and use of a fishbone well pattern to improve SAGD's performance in such reservoirs.

Analysis of the effect of mechanical dispersion on production performance of ES-SAGD is important because of its potential effect on the amount of solvent mixed with bitumen. As mentioned in Sec. 2.1, however, the level of dispersivity in SAGD in Athabasca oil sands is an open question. Until the issue is resolved, sensitivity analysis by perturbation of hydrodynamic dispersivities in numerical simulation can provide qualitative knowledge of how such mixing can affect ES-SAGD. Although not shown in this paper, Venkatramani [35] presented an investigation into the effect of input transverse dispersivity on the performance of ES-SAGD. Results showed that transverse dispersion tends to improve cumulative bitumen production and SOR in ES-SAGD in both homogeneous and heterogeneous reservoirs.

Table 9 Cumulative SOR for SAGD and n-C_6 SAGD for the cumulative bitumen production of 98,458 m^3 for realizations in the second case study (Section 3.2). The homogeneous reservoir model is denoted as realization 0. The average increase in SOR due to heterogeneity (Δ_{het}SOR) for SAGD is 4.87; the corresponding value for n-C_6 SAGD is 2.50. The average reduction in SOR due to coinjection of solvent (Δ_{sol}SOR) for the heterogeneous cases is 3.86.

Realization	Time, days (SAGD)	Time, days (n-C_6 SAGD)	SOR (SAGD)	SOR (n-C_6 SAGD)	Δ_{het}SOR (SAGD)	Δ_{het}SOR (n-C_6 SAGD)	Δ_{sol}SOR
0	499.20	398.01	3.51	2.02	0.00	0.00	1.49
6	1433.49	740.78	6.13	3.58	2.62	1.56	2.55
7	2511.51	951.98	9.32	5.23	5.81	3.21	4.09
15	1349.45	661.62	6.32	3.91	2.81	1.90	2.41
17	3555.48	1085.64	10.60	4.70	7.09	2.68	5.90
18	1952.58	905.72	7.49	4.61	3.98	2.59	2.88
20	3010.76	1034.51	10.17	4.84	6.66	2.83	5.33
21	2541.77	835.31	8.80	4.13	5.29	2.11	4.67
33	2180.70	889.11	7.52	4.43	4.01	2.41	3.09
35	1591.08	836.55	6.78	4.33	3.27	2.32	2.44
44	2224.59	838.70	8.50	4.40	4.99	2.38	4.10
50	2975.84	1241.10	10.56	5.56	7.05	3.54	5.00

4 Conclusions

This paper presented an investigation of SAGD and ES-SAGD in highly heterogeneous reservoirs. The relative performance of ES-SAGD to SAGD under stochastically generated heterogeneity was evaluated in terms of cumulative SOR as a function of cumulative bitumen production. The effect of reservoir heterogeneity on cumulative SOR was explained in terms of the interplay among temperature, chamber geometry, and solvent–bitumen mixing near the chamber edge. Conclusions are as follows:

- Simulation results for heterogeneous reservoir models with horizontal and inclined mudstone bodies showed that SOR of n-C_6 SAGD was less sensitive to heterogeneity than that of SAGD. Also, the reduction in SOR by use of solvent was simulated to be more pronounced under reservoir heterogeneity than in a homogeneous reservoir model. The observed advantage of n-C_6 SAGD over SAGD is because of the dilution of bitumen by solvent (i.e., x_{sL}) and lower chamber-edge temperatures. The lowering of operating chamber-edge temperatures alters the geometry of the steam chamber such that the exposed area for conductive heat losses to the overlying formation rocks is reduced. Steam-solvent coinjection can significantly reduce the consumption of steam to meet a specified cumulative bitumen production when mudstone

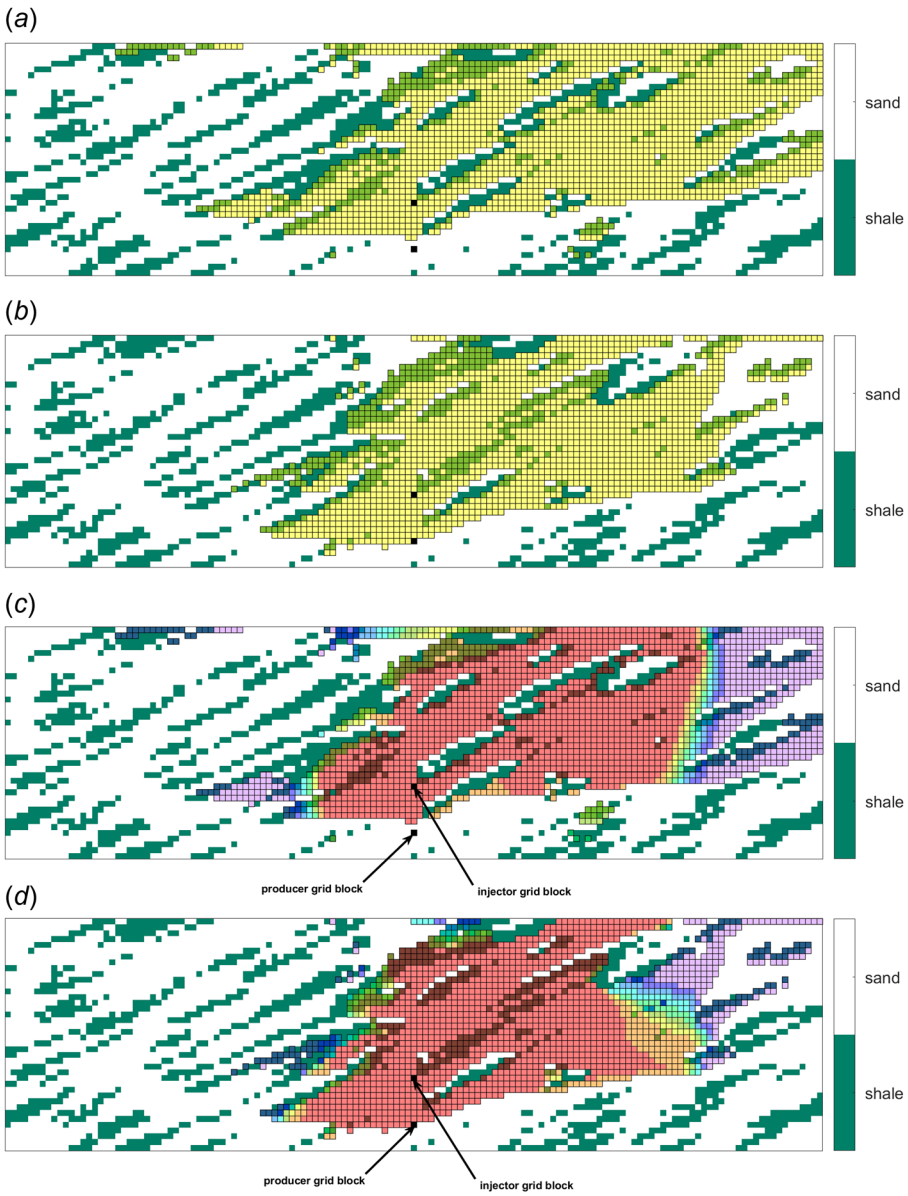

Fig. 8 Steam chambers for SAGD and *n*-C_6 SAGD for realization 17 in the second case study for the cumulative bitumen production of approximately 98,458 m^3 ($0.45V_{SAGD}^{hom}$): (*a*) S_V map for SAGD, (*b*) S_V map for *n*-C_6 SAGD, (*c*) map for concentration of methane in the vapor phase (x_{C1V}) for SAGD, and (*d*) x_{C1V} map for *n*-C_6 SAGD. In (*a*) and (*b*), the grid blocks in the lightly-shaded region correspond to saturations greater than 5%. Maps for x_{C1V} have been provided to delineate the steam chamber. High temperatures within the steam chamber results in the vaporization of methane dissolved in bitumen; the liberated methane then accumulates in the cooler parts of the reservoir, which leads to low values for x_{C1V} inside the steam chamber. In (*c*) and (*d*), the value of x_{C1V} in darkly-shaded grid blocks in the outlined region is lower than 5 mol%. This cumulative bitumen production is met at 3555 days for SAGD and 1086 days for *n*-C_6 SAGD.

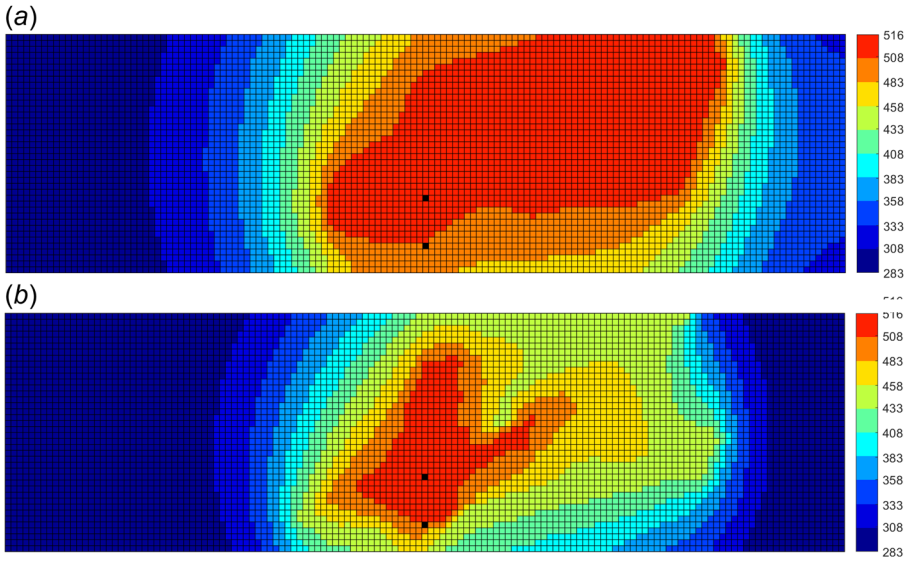

Fig. 9 Maps for temperature (in Kelvin) for SAGD and *n*-C_6 SAGD for realization 17 for the cumulative bitumen production of approximately 98,458 m^3 ($0.45V_{SAGD}^{hom}$) for the second case study; (*a*) SAGD and (*b*) *n*-C_6 SAGD. Injector and producer grid blocks are located in the central grid column and appear black. This cumulative bitumen production is met at 3555 days for SAGD and 1086 days for *n*-C_6 SAGD.

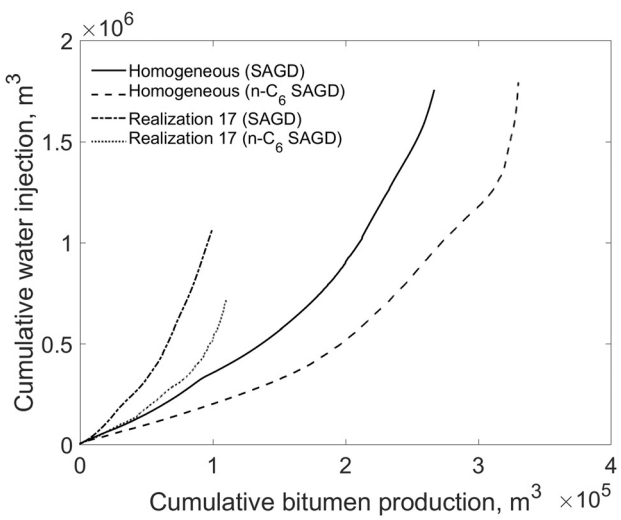

Fig. 10 Cumulative water injection as a function of cumulative bitumen production in SAGD and *n*-C_6 SAGD for the homogeneous reservoir model and realization 17 in the second case study (Sec. 3.2)

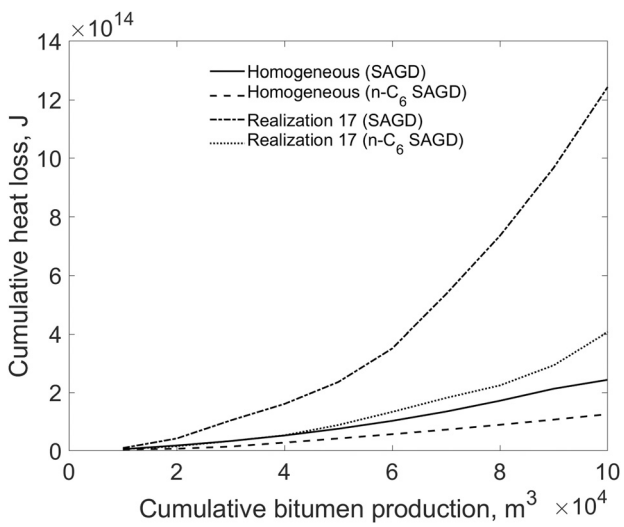

Fig. 11 Cumulative heat loss as a function of cumulative bitumen production in SAGD and *n*-C_6 SAGD for the homogeneous reservoir model and realization 17 in the second case study (Sec. 3.2)

barriers are spatially distributed to moderately impede fluid propagation.

- A larger amount of solvent tends to reside in the oleic phase in heterogeneous cases than in the homogeneous case for a given cumulative bitumen production. The areal span of regions within which x_{sL} exceeds 80 mol% was considerably larger in the presence of mudstone bodies, regardless of the orientation of the mudstone barriers. Reservoir heterogeneity tends to increase the relative magnitude of the dispersive flux in the transverse direction to the convective flux in the longitudinal direction along the edge of a steam chamber in ES-SAGD.
- The simulation case studies considered in this research show that the average reduction in cumulative SOR due to the coinjection of solvent can be higher in the presence of inclined mudstone bodies relative to that under predominantly horizontal mudstone bodies. For instance, at the operating pressure of 35 bars and solvent injection concentration of 2 mol%, the average cumulative SORs for SAGD and ES-SAGD for a cumulative bitumen production of 109,398 m^3, respectively, are 7.28 and 4.38 for heterogeneous models with horizontal barriers, and 8.18 and 4.59 for those with inclined barriers.
- Solvent–bitumen mixing is enhanced under heterogeneity. However, it was observed for some realizations that liquid solvent mixed with bitumen is accumulated in slow-flow (stagnant) regions; i.e., regions of low oleic-phase mobilities and/or regions above laterally extensive mudstone barriers. The retention of solvent in situ in the long term could be reduced by use of a time-variant injection concentration of strategy (VC).

Table 10 Solvent retention ratios for the homogeneous and heterogeneous models in the second case study (inclined mudstone barriers) for the cumulative bitumen production of 98,458 m^3 ($0.45V_{SAGD}^{hom}$). The solvent retention ratio is defined as the ratio of the accumulated solvent volume to the cumulative volume of bitumen produced. These ratios are calculated on the basis of the simulated cumulative bitumen production, solvent injection, and production histories at stock tank conditions.

Realization	Time, days	Accumulated solvent volume, m^3	Solvent retention ratio
0 (homogeneous)	398.01	7229.17	0.07
4	1245.40	27844.34	0.28
6	740.78	19983.71	0.20
7	951.98	13252.27	0.13
15	661.62	16603.76	0.17
17	1085.64	24077.02	0.24
18	905.72	15432.47	0.16
20	1034.51	19625.11	0.20
21	835.31	17903.96	0.18
33	889.11	10693.03	0.11
35	836.55	14475.66	0.15
36	1706.74	17094.11	0.17
44	838.70	18114.18	0.18
50	1241.10	18259.89	0.19

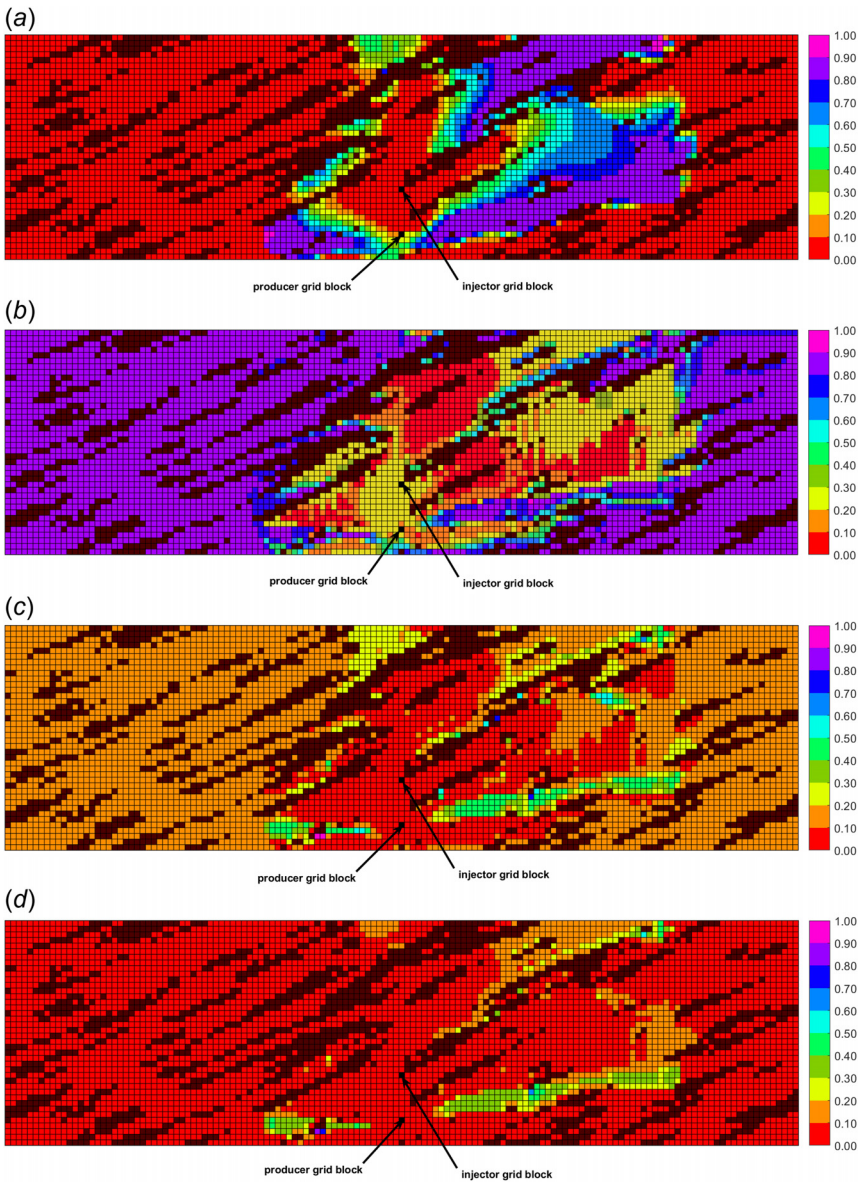

Fig. 12 Property maps for clean sand grid blocks in n-C_6 SAGD for realization 17 from the second case study for the cumulative bitumen production of 98,458 m^3 ($0.45V_{SAGD}^{hom}$); (*a*) x_{sL} map, (*b*) S_L map, (*c*) β_L map, and (*d*) $\beta_L x_{sL}$ map. Mudstone barriers are indicated in the background. This cumulative bitumen production is met at 1086 days.

Acknowledgment

We are grateful to Dr. Juliana Leung at University of Alberta for assisting us with SGeMS. A version of this manuscript was presented at the 2017 Society of Petroleum Engineers (SPE) Heavy Oil Technical Conference in Calgary, Alberta, Canada [50].

Funding Data

We gratefully acknowledge the financial support from Japan Petroleum Exploration Co., Ltd. and Japan Canada Oil Sands, Ltd. Arun Venkat Venkatramani received a travel grant from the Shell enhanced learning fund to present the highlights of this research at the 2017 SPE Heavy Oil Technical Conference in Calgary, Alberta, Canada.

Nomenclature

Roman Symbols

S = saturation
T = temperature
V = volume
W = aqueous phase
x = mole fraction

Greek Symbols

λ = scaling factor for BIP
ω = acentric factor

Subscripts

C_D = dead bitumen
C_1 = methane
L = oleic phase
n-C_6 = normal hexane
s = solvent
V = vapor phase
w = water

Abbreviations

BIP = binary interaction parameter
C = critical constant
EOS = equation of state
ES = expanding solvent
het = heterogeneous case
Hom = homogeneous case
MW = molecular weight
PR = Peng and Robinson
SAGD = steam assisted gravity drainage
SIS = sequential indicator simulation
SOR = steam-oil-ratio
VC = time-variant concentration

References

[1] Keshavarz, M., Okuno, R., and Babadagli, T., 2014, "Efficient Oil Displacement Near the Chamber Edge in ES-SAGD," J. Pet. Sci. Eng., **118**, pp. 99–113.
[2] Rui, Z., Wang, X., and Patil, S., 2018, "A Realistic and Integrated Model for Evaluating Oil Sands Development With Steam Assisted Gravity Drainage Technology in Canada," Appl. Energy, **213**, pp. 76–91.
[3] Zhou, X., Yuan, Q., Peng, X., Zeng, F., and Zhang, L., 2018, "A Critical Review of the CO_2 Huff 'N' Puff Process for Enhanced Heavy Oil Recovery," Fuel, **215**, pp. 813–824.
[4] Ma, Z., Leung, J. Y., and Zanon, S., 2017, "Practical Data Mining and Artificial Neural Network Modeling for Steam-Assisted Gravity Drainage Production Analysis," ASME J. Energy Resour. Technol., **139**(3), p. 032909.
[5] Butler, R., 2001, "Some Recent Developments in SAGD," J. Can. Pet. Technol., **40**(1), pp. 18–22.
[6] Yang, G., and Butler, R. M., 1992, "Effects of Reservoir Heterogeneities on Heavy Oil Recovery by Steam-Assisted Gravity Drainage," J. Can. Pet. Technol., **31**(8), pp. 37–43.
[7] Chen, Q., Gerritsen, M. G., and Kovscek, A. R., 2008, "Effects of Reservoir Heterogeneities on the Steam-Assisted Gravity-Drainage Process," SPE Reservoir Eval. Eng., **11**(5), pp. 921–932.
[8] Yazdi, M. M., and Jensen, J. L., 2014, "Fast Screening of Geostatistical Realizations for SAGD Reservoir Simulation," J. Pet. Sci. Eng., **124**, pp. 264–274.
[9] Wang, C., and Leung, J., 2015, "Characterizing the Effects of Lean Zones and Shale Distribution in Steam-Assisted-Gravity-Drainage Recovery Performance," SPE Reservoir Eval. Eng., **18**(3), pp. 329–345.
[10] Nasr, T. N., Beaulieu, G., Golbeck, H., and Heck, G., 2003, "Novel Expanding Solvent-SAGD Process "ES-SAGD," J. Can. Pet. Technol., **42**(1), pp. 13–16.
[11] Li, W., Mamora, D., and Li, Y., 2011, "Light-and Heavy-Solvent Impacts on Solvent-Aided-SAGD Process: A Low-Pressure Experimental Study," J. Can. Pet. Technol., **50**(4), pp. 19–30.
[12] Li, W., Mamora, D., and Li, Y., 2011, "Numerical Investigation of Potential Injection Strategies to Reduce Shale Barrier Impacts on SAGD Process," J. Can. Pet. Technol., **50**(3), pp. 57–64.
[13] Jha, R. K., Kumar, M., Benson, I., and Hanzlik, E., 2013, "New Insights Into Steam/Solvent- Coinjection-Process Mechanism," SPE J., **18**(5), pp. 867–877.
[14] Keshavarz, M., Okuno, R., and Babadagli, T., 2015, "Optimal Application Conditions for Steam/Solvent Coinjection," SPE Reservoir Eval. Eng., **18**(1), pp. 20–38.
[15] Khaledi, R., Boone, T. J., Motahhari, H. R., and Subramanian, G., 2015, "Optimized Solvent for Solvent Assisted-Steam Assisted Gravity Drainage (SA-SAGD) Recovery Process," SPE Heavy Oil Technical Conference, Paper No. SPE 174429-MS.
[16] Venkatramani, A., and Okuno, R., 2017, "Compositional Mechanisms in Steam-Assisted Gravity Drainage and Expanding-Solvent Steam-Assisted Gravity Drainage With Consideration of Water Solubility in Oil," SPE Reservoir Eval. Eng., **20**(3), pp. 681–697.
[17] Li, W., and Mamora, D., 2010, "Drainage Mechanism of Steam With Solvent Coinjection Under Steam Assisted Gravity Drainage (SAGD) Process," CPS/SPE International Oil and Gas Conference and Exhibition in China, Beijing, China, June 8–10, SPE Paper No. SPE 130802-MS.
[18] Faradonbeh, M. R., Harding, G., and Abedi, J., 2017, "Semianalytical Modeling of Steam/Solvent Gravity Drainage of Heavy Oil and Bitumen: Unsteady-State Model With Curved Interface," SPE Reservoir Eval. Eng., **20**(1), pp. 134–148.
[19] Naderi, K., and Babadagli, T., 2016, "Solvent Selection Criteria and Optimal Application Conditions for Heavy-Oil/Bitumen Recovery at Elevated Temperature: A Review and Comparative Analysis," ASME J. Energy Resour. Technol., **138**(1), p. 012904.
[20] Amani, M. J., Gray, M. R., and Shaw, J. M., 2013, "Phase Behavior of Athabasca Bitumen Water Mixtures at High Temperature and Pressure," J. Supercritical Fluids, **77**, pp. 142–152.
[21] Amani, M. J., Gray, M. R., and Shaw, J. M., 2013, "Volume of Mixing and Solubility of Water in Athabasca Bitumen at High Temperature and Pressure," Fluid Phase Equilib., **358**, pp. 203–211.
[22] Brunner, E., 1990, "Fluid Mixtures at High Pressures IX. Phase Separation and Critical Phenomena in 23 (n-Alkane + Water) Mixtures," J. Chem. Thermodyn., **22**(4), pp. 335–353.
[23] Brunner, E., Thies, M. C., and Schneider, G. M., 2006, "Fluid Mixtures at High Pressures: Phase Behavior and Critical Phenomena for Binary Mixtures of Water With Aromatic Hydrocarbons," J. Supercritical Fluids, **39**(2), pp. 160–173.
[24] Sheng, K., Okuno, R., and Wang, M., 2017, "Water-Soluble Solvent as an Additive to Steam for Improved SAGD," Heavy Oil Technical Conference, Calgary, AB, Canada, Feb. 15–16, SPE Paper No. SPE 184983-MS.
[25] Mohebati, M. H., Maini, B. B., and Harding, T. G., 2012, "Numerical-Simulation Investigation of the Effect of Heavy-Oil Viscosity on the Performance of Hydrocarbon Additives in SAGD," SPE Reservoir Eval. Eng., **15**(2), pp. 165–181.
[26] Ji, D., Dong, M., and Chen, Z., 2015, "Analysis of Steam–Solvent–Bitumen Phase Behavior and Solvent Mass Transfer for Improving the Performance of the ES-SAGD Process," J. Pet. Sci. Eng., **133**, pp. 826–837.
[27] Adepoju, O. O., Lake, L. W., and Johns, R. T., 2013, "Investigation of Anisotropic Mixing in Miscible Displacements," SPE Reservoir Eval. Eng., **16**(1), pp. 85–96.
[28] Adepoju, O. O., Lake, L. W., and Johns, R. T., 2015, "Anisotropic Dispersion and Upscaling for Miscible Displacement," SPE J., **20**(3), pp. 421–432.
[29] Connolly, M., and Johns, R. T., 2016, "Scale-Dependent Mixing for Adverse Mobility Ratio Flows in Heterogeneous Porous Media," Transp. Porous Media, **113**(1), pp. 29–50.
[30] Computer Modeling Group, 2011, *STARS Version 2011-16 User Guide*, CMG, Calgary, AB, Canada.
[31] Remy, N., 2005, "S-GeMS: The Stanford Geostatistical Modeling Software: A Tool for New Algorithms Development," *Geostatistics Banff*, Springer, Dordrecht, The Netherlands, pp. 865–871.
[32] Deutsch, C. V., 2010, "Estimation of Vertical Permeability in the McMurray Formation," J. Can. Pet. Technol., **49**(12), pp. 10–18.
[33] Garmeh, G., 2010, "Investigation of Scale Dependent Dispersivity and Its Impact on Upscaling Miscible Displacements," Ph.D. thesis, The University of Texas at Austin, Austin, TX.
[34] Garmeh, G., and Johns, R. T., 2010, "Upscaling of Miscible Floods in Heterogeneous Reservoirs Considering Reservoir Mixing," SPE Reservoir Eval. Eng., **13**(5), pp. 747–764.
[35] Venkatramani, A., 2017, "Steam-Solvent Coinjection for Bitumen Recovery Under Reservoir Heterogeneity With Consideration of Water Solubility in Oil," Ph.D. thesis, The University of Alberta, Edmonton, AB, Canada.
[36] Lake, L. W., and Hirasaki, G. J., 1981, "Taylor's Dispersion in Stratified Porous Media," SPE J., **21**(4), pp. 459–468.

[37] Gelhar, L. W., Welty, C., and Rehfeldt, K. R., 1992, "A Critical Review of Data on Field-Scale Dispersion in Aquifers," Water Resour. Res., **28**(7), pp. 1955–1974.
[38] Grane, F. E., and Gardner, G. H. F., 1961, "Measurements of Transverse Dispersion in Granular Media," J. Chem. Eng. Data, **6**(2), pp. 283–287.
[39] Alkindi, A. S., Al-Wahaibi, Y. M., and Muggeridge, A. H., 2011, "Experimental and Numerical Investigations Into Oil Drainage Rates During Vapor Extraction of Heavy Oils," SPE J., **16**(2), pp. 343–357.
[40] Kumar, A., 2016, "Characterization of Reservoir Fluids Based on Perturbation From n-Alkanes," Ph.D. thesis, The University of Alberta, Edmonton, AB, Canada.
[41] Peng, D. Y., and Robinson, D. B., 1976, "A New Two-Constant Equation of State," Ind. Eng. Chem. Fundam., **15**(1), pp. 59–64.
[42] Robinson, D. B., and Peng, D. Y., 1978, "The Characterization of the Heptanes and Heavier Fractions for the GPA Peng-Robinson Programs," Gas Processors Association Research, Tulsa, OK, Report No. RR-28.
[43] Kumar, A., and Okuno, R., 2015, "Direct Perturbation of the Peng-Robinson Attraction and Covolume Parameters for Reservoir Fluid Characterization," Chem. Eng. Sci., **127**, pp. 293–309.
[44] Venkatramani, A., and Okuno, R., 2015, "Characterization of Water Containing Oil Using an EOS for Steam Injection Processes," J. Natural Gas Sci. Eng., **26**, pp. 1091–1106.
[45] Coats, K. H., and Smith, B. D., 1964, "Dead-End Pore Volume and Dispersion in Porous Media," SPE J., **4**(1), pp. 73–84.
[46] Dai, K. K., and Orr, F. M., Jr, 1987, "Prediction of CO2 Flood Performance: Interaction of Phase Behavior With Microscopic Pore Structure Heterogeneity," SPE Reservoir Eng., **2**(4), pp. 531–542.
[47] Zhang, B., and Okuno, R., 2015, "Modeling of Capacitance Flow Behavior in EOS Compositional Simulation," J. Pet. Sci. Eng., **131**, pp. 96–113.
[48] Musial, G., Labourdette, R., Franco, J., and Reynaud, J. Y., 2013, "Modeling of a Tide-Influenced Point-Bar Heterogeneity Distribution and Impacts on Steam-Assisted Gravity Drainage Production: Example From Steepbank River, McMurray Formation, Canada," AAPG Stud. Geol., **64**, pp. 545–564.
[49] Zhou, X., Zeng, F., and Zhang, L., 2016, "Improving Steam-Assisted Gravity Drainage Performance in Oil Sands With a Top Water Zone Using Polymer Injection and the Fishbone Well Pattern," Fuel, **184**, pp. 449–465.
[50] Venkatramani, A., and Okuno, R., 2017, "Steam-Solvent Coinjection Under Reservoir Heterogeneity: Should ES-SAGD Be Impelemented for Highly Heterogeneous Reservoirs?," SPE Heavy Oil Technical Conference, Calgary, AB, Canada, Feb. 15–16, SPE Paper No. SPE 185001-MS.